This is the accepted manuscript made available via CHORUS. The article has been published as:

Singlets lead to photogeneration in C_{60}-based organic heterojunctions

Kevin J. Bergemann, Xiao Liu, Anurag Panda, and Stephen R. Forrest

Phys. Rev. B **92**, 035408 — Published 6 July 2015

DOI: 10.1103/PhysRevB.92.035408

Singlets Lead to Photogeneration in C_{60}-based Organic Heterojunctions

Kevin J. Bergemann[1], Xiao Liu[2], Anurag Panda[3], and Stephen R. Forrest[1,2,3]

[1]*Department of Physics, University of Michigan, Ann Arbor, MI, 48109 USA*

[2]*Department of Electrical Engineering and Computer Science, University of Michigan, Ann Arbor, MI, 48109 USA*

[3]*Department of Materials Science and Engineering, University of Michigan, Ann Arbor, MI, 48109 USA*

Abstract

Two independent and direct measurements of exciton transport in the fullerene C_{60} unambiguously indicate that singlets are responsible for energy transport and ultimately charge generation in organic photovoltaic cells. The singlet exciton diffusion length, L_D, was measured using fits to the external quantum efficiency of planar heterojunction photovoltaics, and via C_{60} fluorescence, giving a mean value of 34 ± 3 nm. Direct measurement of the C_{60} singlet state transient fluorescence decay gives a lifetime of 590 ± 10ps, from which we infer a diffusivity of 0.020 ± 0.004 cm^2/s. This is at least ten times that typical for organics, which we attribute to the spherical symmetry of the C_{60} molecule that promotes highly efficient exciton transfer. Further, L_D is used to determine that the C_{60} energy gap is 18 ± 5 meV larger than the analogous fullerene, C_{70}.

I. Introduction

Absorption of a photon in an organic semiconductor results in the formation of a bound electron-hole pair, or exciton. Organic photovoltaic (OPV) cells employ a donor-acceptor heterojunction where excitons dissociate into free charges [1], in contrast to inorganic semiconductors where charge is directly generated by a band-to-band excitation without an intermediate excitonic state [2]. The exciton diffusion length, corresponding to the characteristic distance travelled prior to its recombination, is therefore a fundamental parameter of all organic semiconductors that depends on both the microscopic and macroscopic natures of optically active organic materials [3], and ultimately influences the design of the devices such as OPV cells [4,5].

The fullerene, C_{60}, the most commonly used acceptor in OPVs, has been shown to have a relatively long exciton diffusion length of $L_D \approx 40$ nm, compared to other donors and acceptors whose L_D typically ranges between 5 nm and 10 nm [4]. This occurs despite minimal spectral overlap between C_{60} absorption and the weak C_{60} emission, leading to inefficient Förster energy transfer. There are two competing theories for the origin of this exceptionally long L_D that both agree on the importance of molecular symmetries in C_{60} in forbidding optical transitions from the lowest energy singlet (total spin quantum number S=0) exciton state [6,7]. The C_{60} molecule consists of 60 carbon atoms arranged in 12 five-membered rings and 20 six-membered rings. There are 1812 possible isomers of this structure, but the most stable and only one observed obeys the "isolated pentagons" rule, where each five-membered ring is completely surrounded by six-member rings [6]. This molecular configuration belongs to the icosahedral (I_h) symmetry group, resulting in dipole-forbidden transitions from the lowest energy singlet level (S_1) to the ground state.

The primary differences in the theories for how the dipole-forbidden transitions lead to the long L_D lies in the exciton spin symmetry [1,2,8]. Photogenerated excitons are primarily antisymmetric singlets, but can transfer to spin-symmetric triplet states (S=1) via intersystem crossing. Then the forbidden optical transition might increase the intersystem crossing (ISC) rate, resulting in a triplet population that is expected to have a large L_D due to natural lifetimes of milliseconds or longer. However, no systematic evidence for a larger L_D for singlets in organics compared to triplets has been reported [4,9]. Alternatively, the forbidden transition may simply result in long-lived singlets without involving ISC. Here we add a third explanation, that the excitons transfer between C_{60} molecules is enhanced by their spherical symmetry which depends on the relative spatial orientation of the donor and acceptor molecule [10–12]. Its high efficiency leads to an exceptionally high exciton diffusivity within the films .

The ambiguity in the source of energy transport in C_{60} arises from the difficulties presented by the very low oscillator strength of the singlet transition. Singlet diffusion lengths are accurately determined by characterizing the photoluminescence excitation (PLE) fluorescence spectrum generated by singlet recombination [4,5]. Due to its forbidden singlet dipole transition, C_{60} has extremely weak PL except at low temperatures [13–15] or high excitation intensities [15,16], rendering these techniques impractical. Early attempts to determine the L_D of the fullerenes have therefore employed the indirect and inferential approach of modeling OPV performance by fitting the device external quantum efficiency (*EQE*) [1,8], or by inserting thin exciton blocking layers into the C_{60} [17]. More recently, measurements employing time-resolved microwave conductance [2] and transient absorption in C_{60}-based heterostructures [18] have resulted in reports of L_D varying from 7 nm to 40 nm. However, these

studies had difficulty determining the spin symmetry of the excitation. Furthermore, the large range in measured diffusion lengths leads to uncertainty in interpreting those results [1].

To clarify the mechanisms of energy transfer, we study exciton diffusion in C_{60} by two independent methods. A spin-independent L_D measurement is extracted from fits to the *EQE* spectrum of C_{60} incorporated in C_{60}/tetraphenyldibenzoperiflanthene (DBP) [19] planar heterojunction photovoltaic cells [1,8]. The very low intensity room-temperature steady-state C_{60} PL is also used to unambiguously measure the singlet exciton diffusion length using spectrally-resolved photoluminescence quenching (SR-PLQ) [4,5]. Furthermore, the photoluminescence is shown to originate from the singlet state by measurements of its PL spectrum and fluorescent lifetime. To our knowledge, this is the first transient measurement of the C_{60} lifetime in thin films at room temperature, and it allows for a comparision with the previously reported singlet lifetime of C_{60} in a dilute solution [20].

The properties of C_{60} are further examined using the related fullerene, C_{70}, as a fluorescent probe layer placed in contact with C_{60}. Excitons freely diffuse between C_{70} and C_{60} due to the close match between their highest occupied molecular orbital (HOMO) and lowest unoccupied MO (LUMO) energies [21]. The reduced symmetry of C_{70} gives rise to differences in the absorption spectra and emission intensity compared with C_{60}, allowing for their selective excitation and emission [6,7]. Then, SR-PLQ is used once again to treat exciton diffusion between these materials with different L_D and exciton lifetime, τ. Using this measurement approach, we infer that the energy gap of C_{60} is 18 ± 5 meV larger than C_{70}.

The paper is organized as follows: the following discussion on theory describes our approach to the model of excitons diffusion. Specific film structures, growth and measurement

procedures are described in Sec. III, with results provided in Sec. IV. Our analysis of the data is the subject of Sec. IV where we identify the source of energy transport in C_{60} thin films, followed by conclusions in Sec. V.

II. Theory

Most treatments of exciton diffusion consider only ideal blocking or quenching interfaces, whereby excitons are perfectly reflected back into the material, or are quenched with unity efficiency [1,4,5,8]. Here, we extend the analysis to consider partially blocking or quenching interfaces, as well as to treat exciton diffusion between materials with identical HOMO-LUMO energy gaps but different L_D and τ, as well as the effects of small (~kT, where k is the Boltzmann constant and T is the temperature) energy gap differences on exciton diffusion between such materials. The measurement of L_D via SR-PLQ is based on the steady-state exciton diffusion equation:

$$L_D^2 \frac{\partial^2 n}{\partial x^2} - n + \tau G(x) = 0 \qquad (1)$$

where n is the exciton density generated by the incident PL pump beam, and $G(x)$ is the generation rate at position x. Ideal blocking and quenching interfaces of the material under study are represented by the boundary conditions [4] of $\partial n / \partial x\big|_{x=0} = 0$ and $n(0) = 0$, respectively. The diffusion equation is solved for the case of two identical, semi-infinite layers with either a blocking or a quenching boundary condition at $x = 0$, excited by an exponentially decaying optical field following $G(x) = I_0 \exp(-\alpha x)$, where I_0 is the incident illumination intensity (see Fig. 1a). The ratio of the total exciton population in the two samples is: [4]

$$\eta(\lambda) = \frac{\int_0^\infty n_B(x)dx}{\int_0^\infty n_Q(x)dx} = \alpha'(\lambda)L_D + 1 \qquad (2)$$

where $\alpha' = \alpha / \cos\theta_r$ is the absorption coefficient of the material at wavelength, λ, corrected for the angle of refraction, θ_r, in the layer. The subscript B (Q) indicates a blocking (quenching) layer capping the material under test. Since the PL intensity of a layer is directly proportional to its exciton population, η is also the ratio of the PL of two identical layers with blocking or quenching boundary conditions. Then L_D is calculated by fitting η over a range of λ.

Since the luminescence of C_{60} is so weak, we can place a layer of C_{70} with its nearly identical highest occupied molecular orbital (HOMO) and lowest unoccupied MO (LUMO) adjacent to the C60. Then we can observe spectrally resolved fluorescence from C_{70} as an indicator of the presence of excitons in C_{60}. In this case, C_{70} acts as a *sensitizer* from which we can infer the exciton dynamics of the C_{60}. For analytical purposes, we assume a semi-infinite layer of material 1 (C_{70}) with an interlayer (thickness, d) of material 2 (C_{60}) separating it from a blocking or quenching boundary, as shown in Fig. 1b. The interface between the materials is located at x=0, and the other side of the interlayer is at $x = -d$. We further assume that layer 1 is luminescent while layer 2 is transparent and non-luminescent. In this case, the boundary conditions between the two materials are:

$$\frac{L_{D1}^2}{\tau_1}\frac{\partial n_1}{\partial x}\bigg|_{x=0} = \frac{L_{D2}^2}{\tau_2}\frac{\partial n_2}{\partial x}\bigg|_{x=0}, \text{ or alternatively} \qquad \frac{L_{D1}}{L_{D2}}\xi\frac{\partial n_1}{\partial x}\bigg|_{x=0} = \frac{\partial n_2}{\partial x}\bigg|_{x=0} \qquad (3)$$

and

$$n_1(0) = n_2(0) \qquad (4)$$

where $\xi = \frac{L_{D2}/L_{D1}}{\tau_2/\tau_1}$. These boundary conditions can be used to solve Eq. (1) for a relationship analogous to Eq. (2) that can be fit to yield L_{D2}. Calculating η for a blocking or a quenching boundary at $x = -d$ gives:

$$\eta(\lambda) = \left(\frac{\alpha_1' L_{D1} \xi}{\xi + \tanh\left(L_{D2}/d\right)} + 1 \right) \Bigg/ \left(\frac{\alpha_1' L_{D1} \xi}{\xi + \coth\left(L_{D2}/d\right)} + 1 \right) \tag{5}$$

This reduces to Eq. (2) in the limit of $d = 0$, and to $\eta \to 1$ for $d \to \infty$.

The number of fitting parameters in Eq. (5) can be reduced by a direct measurement of the ratio, ξ. This requires a method for treating non-ideal blocking or quenching interfaces, such as the boundary between two fullerenes (C_{60} and C_{70}) where both the exciton population and its first derivative are non-zero. For this, we introduce the relative blocking efficiency, $\phi = n(0)/n_B$, where as above, n_B is the exciton density at the interface with an ideal blocking layer. Thus, $\phi = 1$ for a perfectly blocking interface, and $\phi = 0$ for a perfect quencher. Solving Eq. (2) using two non-ideal blockers (1 and 2) gives:

$$\eta = \frac{\phi_1 \alpha' L_D + 1}{\phi_2 \alpha' L_D + 1} \tag{6}$$

It is possible to measure L_D separately with Eq. (2), and to determine ϕ_2 by using an ideal blocker or quencher, allowing ϕ_1 of an arbitrary layer to be calculated from η.

The exciton population at a non-ideal interface can also be expressed in terms of ξ, which is calculated based on a direct measurement of ϕ. For an interface between two materials with identical HOMO and LUMO energies at $x = 0$ where material 1 is a finite layer with a blocking

boundary condition at x = -d and a uniform generation rate $G(x) = G_0$, while material 2 is a semi-infinite layer with no absorption (i.e. G=0), the population at the interface using Eqs. (3) and (4) is:

$$n(0) = \frac{\tau_1}{L_{D1}^2} G_0 \left[1 - \frac{1}{\xi \tanh\left(d / L_{D1} \right) + 1} \right]. \tag{7}$$

The population in material 1 for a perfectly blocking interface is: $n_B(0) = (\tau_1 / L_{D1}^2) G_0$. Using this expression and Eq. (7), and assuming $d > 2L_{D1}$, then: $\phi = \xi/(\xi+1)$. If L_{D2} is unknown, it can be obtained using Eq. (5).

Once L_{D2} is determined (i.e. using SR-PLQ), this method can be further extended to examine differences between the HOMO-LUMO energy gaps of the material and its sensitizer. For example, when the energy gap of the materials differ by ~kT, the heterojunction becomes slightly blocking for excitons moving against the energy gradient. Excitons incident on the interface from the smaller energy gap material will have a reduced probability of transfer given by the Miller-Abrahams model: [22,23]

$$P_{1\to 2} = \begin{cases} \exp\left(-\dfrac{\varepsilon_1 - \varepsilon_2}{kT} \right) & \varepsilon_1 < \varepsilon_2 \\ 1 & \varepsilon_1 \geq \varepsilon_2 \end{cases} \tag{8}$$

where $P_{1\to 2}$ is the transfer probability from material 1 to 2, and ε_1 and ε_2 are their respective energy gaps. The exciton distribution in the two materials is calculated by taking a weighted average of solutions to Eq. (1) for a perfectly blocking interface, and a perfectly energy-matched

interface based on $P_{1\to 2}$. The new exciton distribution is then used in Eq. (5), allowing the ratio to be fit to the heterojunction energy offset, $\Delta\varepsilon = \left|\varepsilon_1 - \varepsilon_2\right|$.

III. Experimental

All samples were deposited in high vacuum (<10^{-6} torr), with fullerenes and DBP source materials purified once via vacuum thermal gradient sublimation prior to use. Samples for SR-PLQ measurements used structure A in Table 1. Samples for the C_{60} interlayer measurements used structure B, and blocking efficiency measurements used structure C. Both 310 nm and 60 nm thick layers of C_{60} were tested for structure A, and gave similar results. As expected, the thicker layer had a much stronger PL signal and hence provided the more accurate values reported here. The 20 nm thick C_{60} layer in structure C prevents interactions between excitons in C_{70} and the top surface of the C_{60} layer. The luminescent C_{60} layer was deposited simultaneously in all three samples. Bathophenanthroline (Bphen) was used as an exciton blocker and N,N′-Di-[(1-naphthyl)-N,N′-diphenyl]-1,1′-biphenyl)-4,4′-diamine (NPD) was the exciton quencher.

The OPV used structure D in Table 1. A device area of 1 mm^2 was defined by a shadow mask during metal cathode deposition. The *EQE* was measured as previously reported [24]. Fits to the *EQE* were performed using the method of Peumans, et al. [1] on C_{60} in its absorption range of λ=380 nm to 520 nm. The PL measurements were taken in a high purity N_2 atmosphere at a pump incidence angle of θ=30°. The intensity was measured at 60° from normal at λ=750 nm for C_{60} and λ=685 nm for C_{70}. Fits to the PL data were performed by calculating η via Eq. (1), with G(x) obtained via the transfer matrix method [5]. All optical constants and thicknesses were

measured using a variable angle spectroscopic ellipsometer. All measurements were taken at room temperature.

Transient PL measurements were performed on 80 nm thick C_{60} samples excited at λ = 480 nm in the middle of the singlet charge transfer state absorption line [25] with 150 fs pulses at a 1 kHz repetition rate using the output from a a Ti:Sapphire laser-pumped optical parametric amplifier. The pulse energy was kept at 2.1 nJ - 4.9 nJ to minimize bi-exciton quenching.

IV. Results

The PL spectra of C_{60} thin films at room temperature and 20 K are shown in Fig. 2. The transient PL and a single exponential fit convolved with the instrument response are shown in Fig. 2, inset, giving a C_{60} singlet lifetime of 590 ± 10 ps.

The *EQE* spectrum of a planar DBP/C_{60} OPV (structure D) is shown in Fig. 3 (inset). A fit to the *EQE* in the region of C_{60} absorption [1] yields L_D = 32 ± 2 nm. The SR-PLQ measurements of C_{60} (structure A) give L_D = 36 ± 2 nm, with sample PLE data shown in Fig. 3. Fits to the ratio of these data using Eq. (2) are shown in Fig. 4 (circles). The PL emission was measured at λ=750 nm, corresponding to C_{60} fluorescence [21]. The PLE spectral ratios from SR-PLQ data of the C_{70} film and C_{60} interlayer structures for C_{70} (structure B) are shown in Fig. 4. Figure 5 shows the spectra of samples in structure C, which are used to calculate the exciton blocking efficiency of C_{70}.

V. Discussion

The PL spectrum in Fig. 2 shows a clear vibronic progression, where the zero phonon feature (ZPL) of singlet transition is visible at approximately λ = 725 nm along with higher-order

vibronic replicas [16]. No triplet phosphorescence emission is visible, and to date no spectroscopic evidence has shown the triplet states from ISC dominantly exist in C_{60} thin films, even at low temperatures. Transient PL further shows that singlet emission from the C_{60} thin film has a lifetime of 590 ± 10ps. This is shorter than the reported singlet lifetime of C_{60} in solvent of 1.17ns [20]. Note that our photoexcitation falls within the range of ~2.1eV to ~3.2eV, whereby either the Frenkel or charge transfer (CT) states are excited [25–27]. Thus, the C_{60} singlet emission can have its origin from either the generation of a CT or Frenkel exciton, although the energy of emission suggests that the rapid transfer from the CT to the Frenkel state is the most likely process. For efficient transfer and emission, the spin symmetry of both states must correspond to the singlet, S=0, state. A similar mixing also occurs in C_{70}, where the allowed Frenkel and CT state absorption overlaps in the range of between 1.88 eV and 3.6 eV [25].

In structure B, sequential transfer from C_{60} to C_{70} and then back to C_{60} is efficient only if spin is conserved during the transfer process. Since emission in C_{70} is due to singlet state, the C_{70} sensitization of C_{60} in structure B, therefore, provides additional evidence for energy transfer via singlets in the latter molecule. The diffusion length measured using a C_{60} interlayer on C_{70} (structure B), was L_D=20 ± 2 nm. This smaller value suggests there is a difference between the energy gaps, $\Delta\varepsilon = |\varepsilon_1 - \varepsilon_2|$, of the two fullerenes. Fitting the ratio of the data in Fig. 4, using Eq. (5) and (8), and L_D = 36 nm gives $\Delta\varepsilon$ = 18 ± 5 meV (Fig. 4), with C_{60} having the wider energy gap. Also, for C_{70}, we find that L_D = 10 ± 1 nm (Fig. 4), consistent with previous reports [28], and the blocking efficiency of C_{60} on C_{70} was □ = 62 ± 6%, using data from structure C in Fig. 5 along with Eq. (6). This corresponds to ξ = 1.6 ± 0.4.

Exciton diffusion lengths measured for C_{60} based on *EQE* and SR-PLQ are consistent with previous measurements by Peumans [1] and Qin [17]. Since the spin-independent *EQE* measurement and the SR-PLQ measurement that depends only on the optical generation of emissive singlets agree with a mean of $L_D = 34 \pm 3$ nm, we conclude that photocurrent due to absorption in the C_{60} layer in OPVs primarily originates from singlets. That is, excitons in both measurements generated on optical absorption result primarily in singlets due to spin selection rules. If triplets play a significant role in energy transport, the *EQE* measurements should give a value for L_D that is the sum of the triplet and singlet diffusion lengths, since excitons would diffuse some distance as singlets before crossing to the triplet manifold. We instead measure the same L_D (within experimental error) through both singlet-only measurements and *EQE* measurements, from which we infer that triplets do not contribute significantly to energy transport and that singlets are the primary source of photocurrent in OPV.

In contrast to our measurement of $L_D = 34 \pm 3$ nm, Fravventura et al. [2] reported singlet excitons with $L_D = 7.1 \pm 0.5$ nm using time-resolved microwave conductance. Lane et al [18] found $L_D = 10 \pm 4$ nm in C_{60} nanostructures. The discrepancies between these values are attributed to differences in C_{60} crystallinity and purity [1]. Also, the very short diffusion lengths contradict considerable work on OPV cells. This suggests that singlet recombination in samples with uncertain purity may occur through defects, hence circumventing the strict quantum mechanical selection rules arising from the C_{60} molecular symmetry.

The importance of purity to the measured L_D is supported by our own work on different batches of C_{60}. Devices using C_{60} with $L_D = 36 \pm 2$ nm yielded the highest OPV efficiencies, suggesting high purity. In contrast, devices made with a separate source batch of C_{60} from the same supplier showed significantly reduced efficiency, and showed $L_D = 20 \pm 2$ nm. All source

materials used in this study were purified using thermal gradient sublimation as above, but reduced purity in the starting material nevertheless results in a 45% reduction in L_D, indicating the importance of using high quality starting materials. Indeed, it has been shown that contamination can lead to C_{60} oligomerization and oxidation, where the reaction products have a significantly reduced τ, and hence L_D compared pure C_{60} [29].

Our measurement of L_D = 34 ± 3 nm and singlet lifetime 590 ± 10 ps yields a calculated diffusivity ($D = L_D^2/\tau$) for C_{60} thin films of 0.020 ± 0.004 cm^2/s, an order of magnitude larger than in most organic semiconductors[4]. We attribute this to the unusual spherical symmetry of the C_{60} molecule. The exciton transfer efficiency is known to depend on the relative orientation of the donor and acceptor molecules [10–12]. The spherical symmetry of C_{60} allows for optimum charge transfer between adjacent molecules independent of their relative orientation. Thus, the large value of D, and not the spin symmetry of the exciton state, leads to the large L_D of C_{60}. Indeed, this close packing arrangement allowed by the unique molecular symmetry of C_{60} is also responsible for the strong CT state absorption.

VI. Conclusions

We find that the photocurrent in optically-excited C_{60} films originates from singlet excitons. Using two different independent techniques, we obtain a mean exciton diffusion length L_D = 34 ± 3 nm. We have further performed measurements of C_{60} fluorescence emission and lifetime in thin films at room temperature, giving a singlet lifetime of 590 ± 10 ps and a corresponding diffusivity of 0.020 ± 0.004 cm^2/s which is at least 10 times higher than most organic molecular species. The long L_D of C_{60} is thus due to high diffusivity caused by the

spherical symmetry of C_{60} that leads to close packing and efficient intermolecular charge transfer We have further employed C_{70} as a fluorescent sensitizer for C_{60} to extract the energy offset of 18 ± 5 meV between the two materials, where the energy gap of C_{60} is the greater of the two. We have developed techniques to include the effects of partially blocking or quenching interfaces on exciton diffusion between materials with only minor differences in energy gaps, but with different L_D and τ. While C_{60} is in itself a uniquely important molecule in organic electronic applications and particularly in OPVs, the techniques introduced here can be used to accurately determine the fundamental materials properties of an expanded class of materials.

Acknowledgments

The authors gratefully acknowledge Prof. Jeramy Zimmerman, Dr. Olga Griffith, and Mr. Quinn Burlingame for useful discussions. This work was partially supported by the Center for Solar and Thermal Energy Conversion at the University of Michigan (Department of Energy, Energy Frontier Research Center, Award No. DE-SC0000957; KJB, measurements, analysis), the Air Force Office of Scientific Research (SRF, analysis, project direction), the SunShot Program of the Department of Energy (XL, spectral measurement), and NanoFlex Power Corp. (AP, analysis).

[1] P. Peumans, A. Yakimov, and S. R. Forrest, J. Appl. Phys. **93**, 3693 (2003).

[2] M. C. Fravventura, J. Hwang, J. W. A. Suijkerbuijk, P. Erk, L. D. A. Siebbeles, and T. J. Savenije, J. Phys. Chem. Lett. **3**, 2367 (2012).

[3] R. R. Lunt, J. B. Benziger, and S. R. Forrest, Adv. Mater. **22**, 1233 (2010).

[4] R. R. Lunt, N. C. Giebink, A. A. Belak, J. B. Benziger, and S. R. Forrest, J. Appl. Phys. **105**, 053711 (2009).

[5] K. J. Bergemann and S. R. Forrest, Appl. Phys. Lett. **99**, 243303 (2011).

[6] G. Orlandi and F. Negri, Photochem. Photobiol. Sci. **1**, 289 (2002).

[7] J. W. Arbogast, A. P. Darmanyan, C. S. Foote, F. N. Diederich, R. L. Whetten, Y. Rubin, M. M. Alvarez, and S. J. Anz, J. Phys. Chem. **95**, 11 (1991).

[8] L. A. A. Pettersson, L. S. Roman, and O. Inganäs, J. Appl. Phys. **86**, 487 (1999).

[9] Y. Shao and Y. Yang, Adv. Mater. **17**, 2841 (2005).

[10] S. Saini, G. Srinivas, and B. Bagchi, J. Phys. Chem. B **113**, 1817 (2009).

[11] K. F. Wong, B. Bagchi, and P. J. Rossky, J. Phys. Chem. A **108**, 5752 (2004).

[12] W. Chen, D.-C. Qi, H. Huang, X. Gao, and A. T. S. Wee, Adv. Funct. Mater. **21**, 410 (2011).

[13] W.-C. Hung, C.-D. Ho, C.-P. Liu, and Y.-P. Lee, J. Phys. Chem. **100**, 3927 (1996).

[14] C. Reber, L. Yee, J. McKiernan, J. I. Zink, R. S. Williams, W. M. Tong, D. A. A. Ohlberg, R. L. Whetten, and F. Diederich, J. Phys. Chem. **95**, 2127 (1991).

[15] E. Shin, J. Park, M. Lee, D. Kim, Y. Doug Suh, S. Ik Yang, S. Min Jin, and S. Keun Kim, Chem. Phys. Lett. **209**, 427 (1993).

[16] V. Capozzi, G. Casamassima, G. F. Lorusso, A. Minafra, R. Piccolo, T. Trovato, and A. Valentini, Solid State Commun. **98**, 853 (1996).

[17] D. Qin, P. Gu, R. S. Dhar, S. G. Razavipour, and D. Ban, Phys. Status Solidi A **208**, 1967 (2011).

[18] P. A. Lane, P. D. Cunningham, J. S. Melinger, G. P. Kushto, O. Esenturk, and E. J. Heilweil, Phys. Rev. Lett. **108**, 077402 (2012).

[19] X. Xiao, J. D. Zimmerman, B. E. Lassiter, K. J. Bergemann, and S. R. Forrest, Appl. Phys. Lett. **102**, 073302 (2013).

[20] D. Kim, M. Lee, Y. D. Suh, and S. K. Kim, J. Am. Chem. Soc. **114**, 4429 (1992).

[21] S. Kazaoui, N. Minami, Y. Tanabe, H. J. Byrne, A. Eilmes, and P. Petelenz, Phys. Rev. B **58**, 7689 (1998).

[22] A. Miller and E. Abrahams, Phys. Rev. **120**, 745 (1960).

[23] I. I. Fishchuk, D. Hertel, H. Bässler, and A. K. Kadashchuk, Phys. Rev. B **65**, 125201 (2002).

[24] J. D. Zimmerman, X. Xiao, C. K. Renshaw, S. Wang, V. V. Diev, M. E. Thompson, and S. R. Forrest, Nano Lett. **12**, 4366 (2012).

[25] S. Kazaoui, N. Minami, Y. Tanabe, H. J. Byrne, A. Eilmes, and P. Petelenz, Phys. Rev. B **58**, 7689 (1998).

[26] T. Tsubo and K. Nasu, Solid State Commun. **91**, 907 (1994)

[27] X. Wei, D. Dick, S. A. Jeglinski and Z. V. Vardeny, Synth, Met. **86**, 2317 (1997)

[28] B. E. Lassiter, J. D. Zimmerman, A. Panda, X. Xiao, and S. R. Forrest, Appl. Phys. Lett. **101**, 063303 (2012).

[29] Q. Burlingame, X. Tong, J. Hankett, M. Slootsky, Z. Chen, and S. R. Forrest, Energy Environ. Sci. **8**, 1005 (2015).

Table 1: Structures used for (A) spectrally-resolved photoluminescence quenching, (B) C_{60} interlayer, and (C) blocking efficiency measurements (blocking (Bl) and quenching (Q) cap layers indicated). Structure (D) is an OPV.

Structure	**Active Layer**	**Interlayer**	**Cap**
A	310 nm C_{60}	None	8 nm BPhen (Bl) 8 nm NPD (Q)
B	80 nm C_{70}	8/13/15 nm C_{60}	8 nm BPhen (Bl) 8 nm NPD (Q)
C	80 nm C_{70}	None	8 nm BPhen (Bl) 8 nm NPD (Q) 20 nm C_{60} (Non-Ideal)

	Anode	**Anode Blocker**	**Donor**	**Acceptor**	**Cathode Blocker**	**Cathode**
D	ITO	10 nm MoO_3	10 nm DBP	40 nm C_{60}	10 nm BPhen	100 nm Ag

Figure Captions

Figure 1. Layering schemes and boundary conditions used in modeling (a) spectrally-resolved photoluminescence quenching (SR-PLQ) and blocking efficiency measurements, and (b) C_{60} interlayer measurements.

Figure 2. Photoluminescence spectra at room temperature and at 20K for an 80 nm thick film of C_{60} deposited onto a Si substrate. Here, ZPL is the zero phonon line, and 1PL, 2PL and 3PL is the progression of phonon replicas as identified in Ref. 10. Inset: Fluorescence decay curve for 80 nm C_{60} thin film at room temperature giving a fluorescence lifetime of 590 ± 10 ps. The fit (red line) to the single exponential decay model convolved with the instrument response function is shown.

Figure 3. Photoluminescence excitation (PLE) data for 310 nm thick C_{60} layers, normalized to maximum peak height of the blocking sample. The C_{60} was capped with a blocking Bphen, or a quenching NPD layer. Samples were excited at a 30° from normal incidence, and emission detected at θ=60° at λ=750 nm. Inset: External quantum efficiency (*EQE*) (squares) for the organic photovoltaic (OPV) structure D. The shaded area indicates the range of C_{60} absorption, and the remainder is the range of DBP absorption. Solid line is a fit to the C_{60} response of *EQE*, giving a diffusion length of L_D = 32 ± 2 nm.

Figure 4. Ratio of photoluminescence excitation (PLE) spectral intensities ($\eta(\lambda)$) and fits using theory in text. Spectrally-resolved photoluminescence quenching (SR-PLQ) was used to fit the data from C_{60} (circles) and C_{70} (downwards-pointing triangles) films, giving L_D = 36 ± 2 nm and L_D = 10 ± 2 nm, respectively. C_{60} interlayers of 8 nm (upwards-pointing triangles) and 15 nm (squares) were fit using intermediate boundary conditions at the interface between the fullerenes, giving L_D = 20 ± 2 nm for both.

Figure 5. Photoluminescence (PL) spectra used to calculate the C_{60} exciton blocking efficiency by C_{70}, yielding □ = 62 ± 6%. Samples were comprised of a 80 nm thick C_{70} layer capped with an 8 nm thick blocking (Bphen) or quenching (NPD) layer, or a 20 nm thick C_{60} cap. Samples were excited at λ=540, where C_{70} has strong absorption and C_{60} does not. Data are normalized to maximum peak height of the blocking sample. Inset: PL excitation (PLE) spectral intensity of an 8 nm thick C_{60} interlayer between an 80 nm thick C_{70} and an 8 nm thick blocking (Bphen) or quenching (NPD) cap layer. Emission was measured at λ=685 nm, corresponding to the peak of the C_{70} singlet exciton absorption. Data are normalized to maximum peak height of the blocking sample.

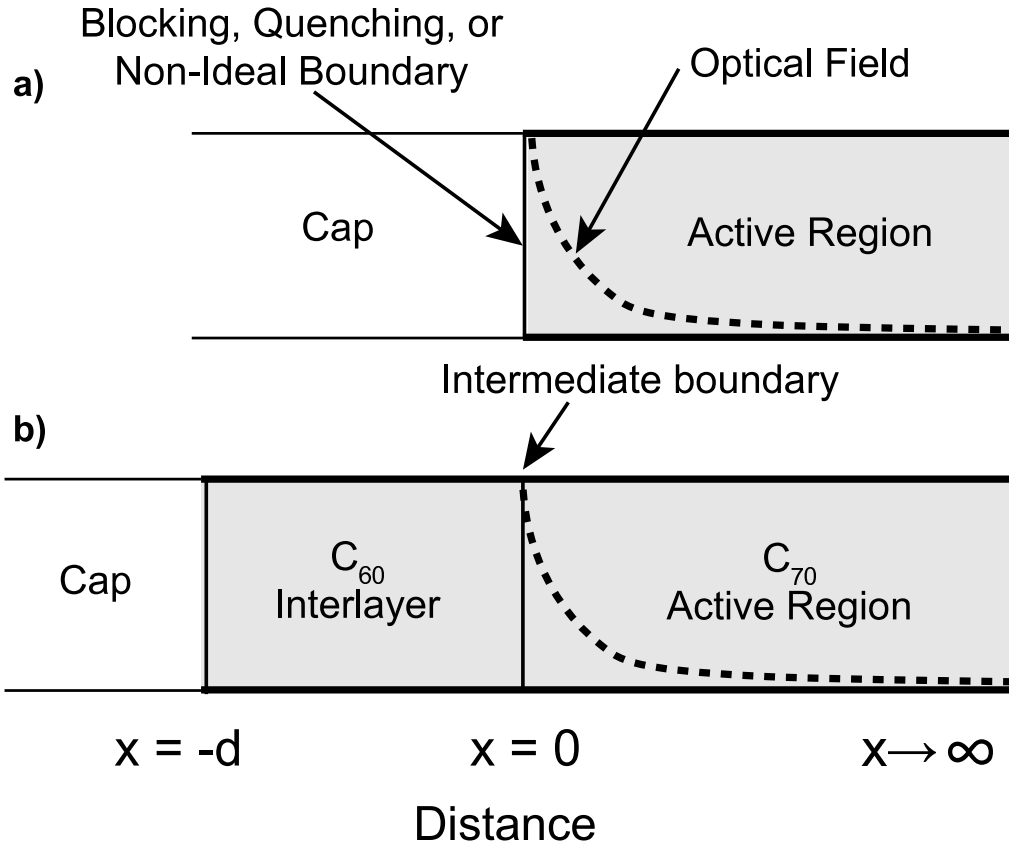

Figure 1 LA15053B 17JUN2015

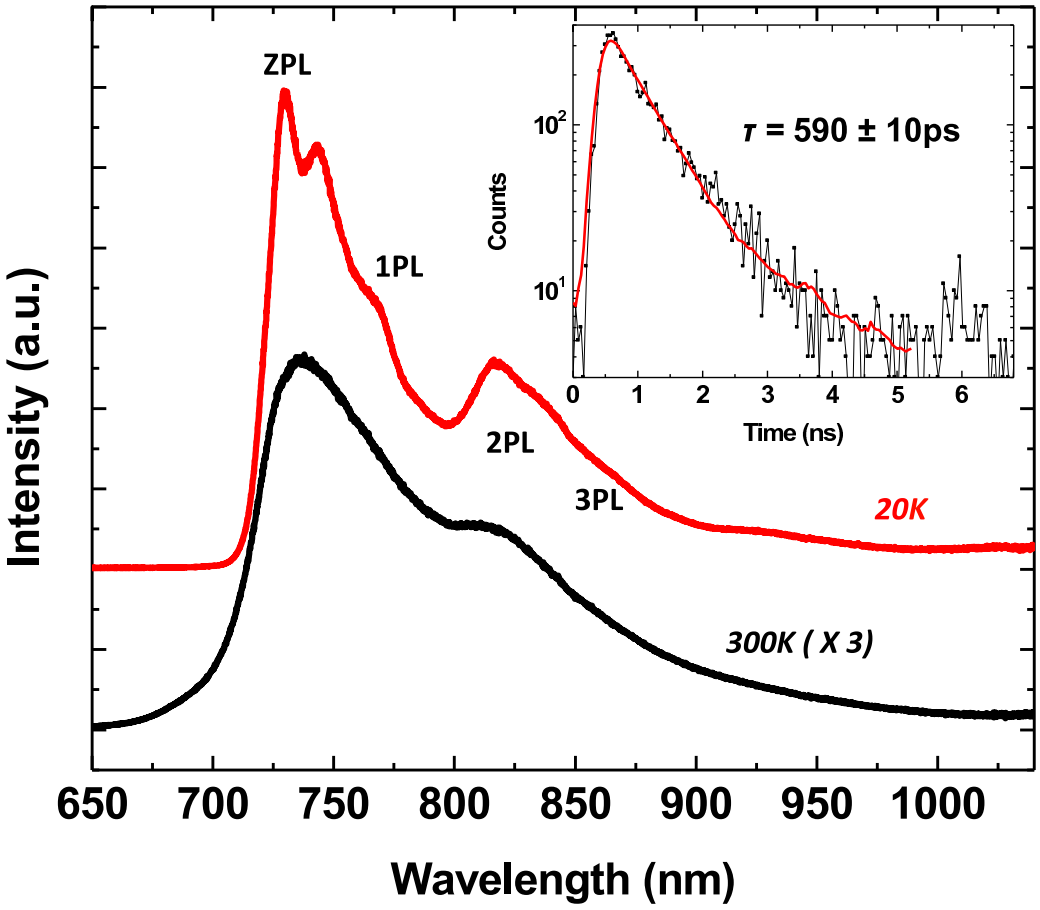

Figure 2 LA15053B 17JUN2015

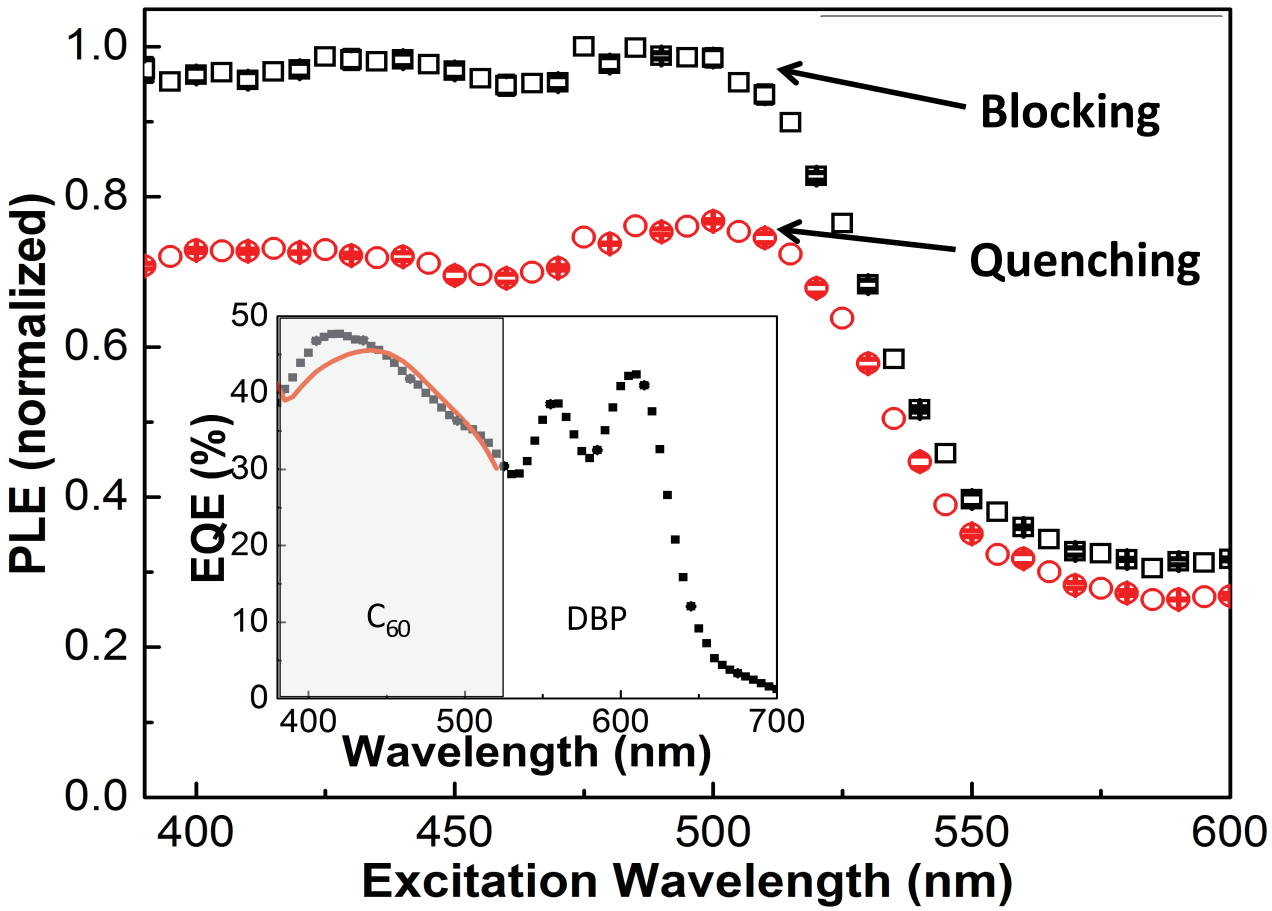

Figure 3 LA15053B 17JUN2015

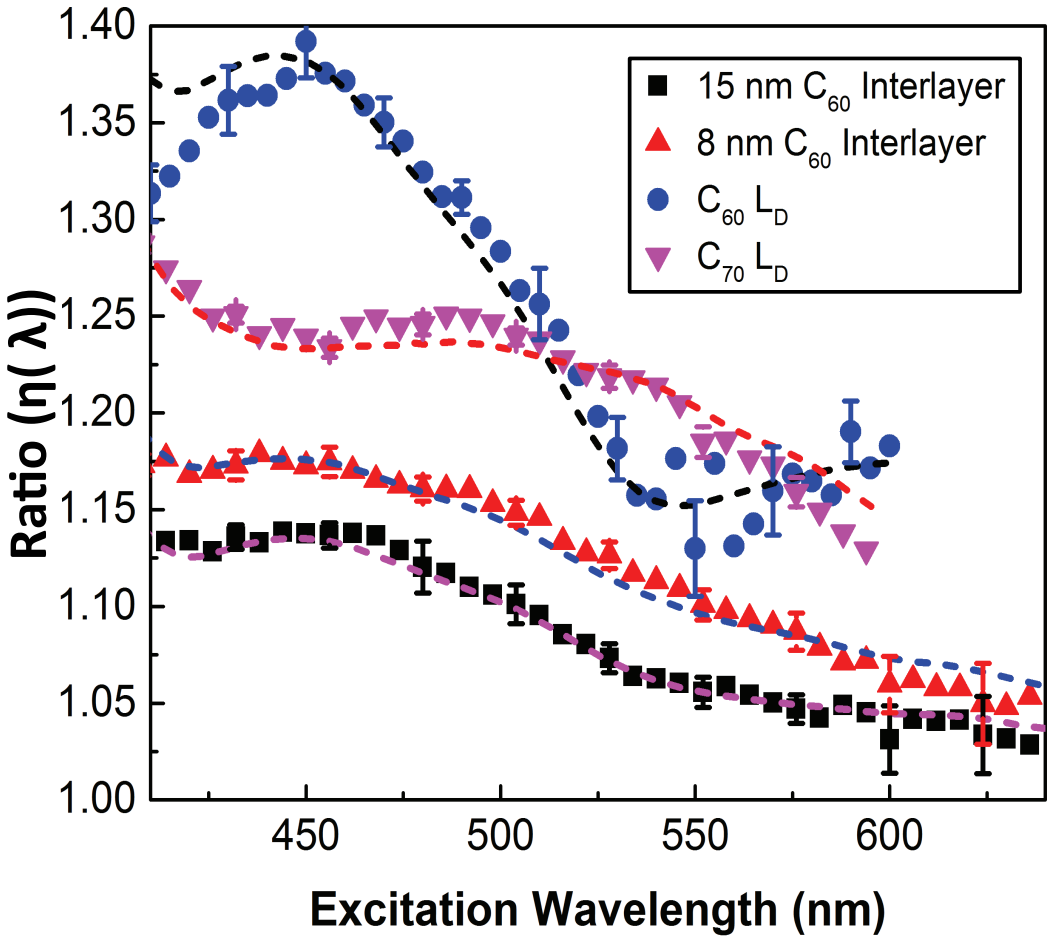

Figure 4 LA15053B 17JUN2015

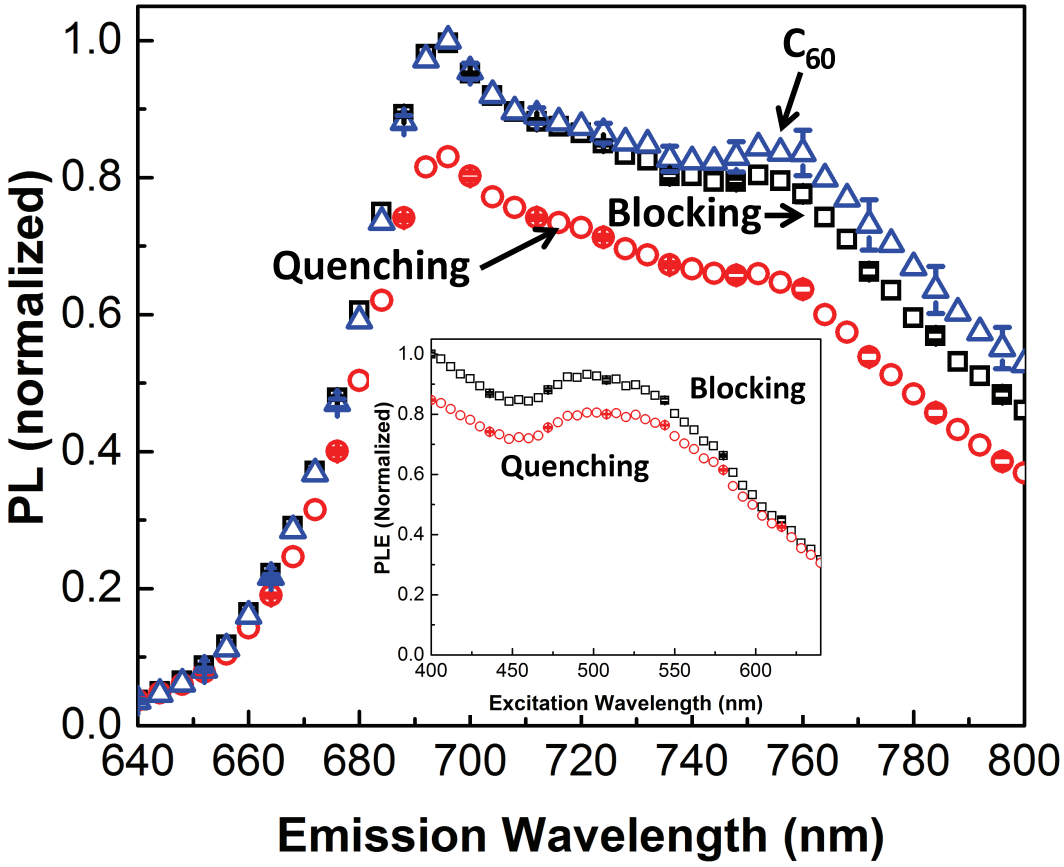

Figure 5 LA15053B 17JUN2015